HHS Public Access

Author manuscript

Magn Reson Med. Author manuscript; available in PMC 2017 May 12.

Published in final edited form as:

Magn Reson Med. 2017 May ; 77(5): 2048–2056. doi:10.1002/mrm.26268.

Pregnant Women Models Analyzed for RF Exposure and Temperature Increase in 3T RF Shimmed Birdcages

Manuel Murbach[1,*], **Esra Neufeld**[1], **Theodoros Samaras**[2], **Juan Córcoles**[3], **Fraser J. Robb**[4], **Wolfgang Kainz**[5], and **Niels Kuster**[1,6]

[1]IT'IS Foundation, Zurich, Switzerland [2]Department of Physics, Aristotle University of Thessaloniki, Thessaloniki, Greece [3]Department of Electronic and Communication Technology, Universidad Autónoma de Madrid (UAM), Escuela Politécnica Superior, Madrid, Spain [4]GE Healthcare, Aurora, OH, USA [5]US Food and Drug Administration (FDA), Center for Devices and Radiological Health (CDRH), Silver Spring, MD, USA [6]Swiss Federal Institute of Technology (ETH), Zurich, Switzerland

Abstract

Purpose—MRI is increasingly used to scan pregnant patients. We investigated the effect of 3 Tesla (T) two-port radiofrequency (RF) shimming in anatomical pregnant women models.

Theory and Methods—RF shimming improves B_1^+ uniformity, but may at the same time significantly alter the induced current distribution and result in large changes in both the level and location of the absorbed RF energy. In this study, we evaluated the electrothermal exposure of pregnant women in the third, seventh, and ninth month of gestation at various imaging landmarks in RF body coils, including modes with RF shimming.

Results—Although RF shimmed configurations may lower the local RF exposure for the mother, they can increase the thermal load on the fetus. In worst-case configurations, whole-body exposure and local peak temperatures—up to 40.8°C—are equal in fetus and mother.

Conclusions—Two-port RF shimming can significantly increase the fetal exposure in pregnant women, requiring further research to derive a very robust safety management. For the time being, restriction to the CP mode, which reduces fetal SAR exposure compared with linear-horizontal polarization modes, may be advisable. Results from this study do not support scanning pregnant patients above the normal operating mode.

Keywords

MRI safety; SAR; RF shimming performance; Virtual Population; thermoregulation

[*]Correspondence to: Manuel Murbach, Ph.D., IT'IS Foundation, Zeughaus-strasse 43, 8004 Zurich. Telephone: 141-44-2459696; Fax: +141-44-2459699; murbach@itis.ethz.ch.

INTRODUCTION

MRI is a powerful, noninvasive imaging technique that is increasingly used to scan pregnant women. MRI offers high soft-tissue contrast, a large field of view (FOV), and larger penetration depths than ultrasound. Among others, abnormal fetal position, brain or body abnormalities, overlying bone, or maternal obesity are considered indications for fetal MRI (1,2). However, absorbed radiofrequency (RF) energy must be very carefully managed, especially as the highly conductive amniotic fluid is not perfused and, thus, has limited capacity for heat dissipation and thermoregulation. Exposure scenarios for two-port (here named I and Q) body coils at 3 Tesla (T) are investigated within this study to assess the local RF exposure and the induced temperature increase in typical imaging landmarks for pregnant women at several gestational stages and for different RF shimming excitations. In contrast to circularly polarized (CP) B_1 fields at 1.5T, the polarization in RF shimmed body coils may become linear with arbitrary polarization angles, which can significantly increase local RF absorption (3).

RF exposure in resonant body coils is controlled using the specific absorption rate (SAR). Limits defined by the corresponding International Electrotechnical Commission (IEC) product standard (4) cover whole-body SAR (wbSAR), head SAR (hdSAR), and partial-body SAR (pbSAR). The local SAR, typically defined as the peak spatial SAR averaged over any 10 g of tissue (psSAR10g), is not limited by the IEC standard for resonant volume coils.

IEC 60601-2-33 (4) currently suggests that pregnant women should be limited to scans performed in the normal operating mode (OM), in which the wbSAR is limited to 2 W/kg (4). The wbSAR limit was reached before the limitations for hdSAR and pbSAR in all investigated scenarios, which are in torso-landmarks around the fetus.

Although limiting the whole-body absorption is believed to provide sufficient protection against whole-body heating of the mother, the local exposures can reach high values. Previous studies limited to CP exposure (5,6) have only estimated psSAR10g values of >20 W/kg in the mother, and >5 W/kg in the fetus. Numerical studies with homogenous pregnant models have resulted in estimations of psSAR10g values in the fetus of up to 8 W/kg at 1.5T, and 5 W/kg at 3T, with maxima at 5 and 9 months of gestation, respectively (7). These values are expected to be considerably higher when RF shimming is included, as investigated in this study.

The RF-induced temperature increase is estimated to result in temperatures higher than 38°C in the fetus when exposure at a constant wbSAR of 2 W/kg is applied for more than 7 min (6). However, as mentioned in the corresponding study, the estimation of temperature based on a static model is problematic, because of frequent movement of the fetus.

For psSAR10g values above the transition zone of approximately 10 to 20 W/kg, the thermoregulation of the local blood flow becomes the dominant factor affecting the peak temperature actually attained (8,9). Thus, the exposure of pregnant women in the normal OM is just at the onset of the local thermoregulation, which is achieved by thermally induced local blood-perfusion increase through vasodilation, also called thermal hyperemia

(8,10). In contrast to whole-body thermal stress, local temperatures may not be adequately perceived by the mother, as humans are limited in their ability to sense heat, eg, in muscle tissue (11), and the capacities for thermo-sensation and regulation in the fetus are widely unknown (12).

In addition to SAR and temperature evaluations, the performance of RF shimming is evaluated in terms of the B_1^+ coefficient of variation ($CV(B_1^+)$) and the average B_1^+ field strength (average $|B_1^+|$) within selected regions of interest (ROI).

METHODS

Anatomical Models and Simulation Setup

The anatomical pregnant human model Ella (at 3, 7, and 9 months of gestation) from the Virtual Population (13,14) was evaluated in five *z*-axis positions (landmarks heart to groin) within generic two-port 3T body coils; a 1.5T coil was added for comparison. Two additional models in which the fetus is positioned head-up (breech) at 7 and 9 months of gestation, as well as a neonate model (infant without its mother), were included. The simulation scenario and anatomical models are depicted in Figure 1, where also five typical imaging landmarks around the fetus are defined with the ROI for each landmark. A minimal distance of 10 mm between the arm and hip was ensured to avoid RF loops. The dielectric and basal thermal tissue properties were assigned according to the comprehensive literature review of Has-gall (www.itis.ethz.ch/database), the recommended dielectric properties of which are largely identical to those proposed by Gabriel et al (15). Identical tissue properties were assigned for fetus and mother, except for the noninflated fetal lung. The effect of age-adjusted properties assessed in (16) was included in the uncertainty budget, with differences in white matter, spinal cord, and bone of up to 68% for adults compared with young age. However, there were insignificant changes (<1%) in the values for SAR and temperature increase when age-adjusted properties were used. For comparison, homogenous fetal tissue properties as used in Hand et al (6) were applied as well.

All models and imaging landmarks were simulated within the reference two-port generic birdcage, which is wide-bore and average in length (128 MHz resonant, band-pass, two-port feed, 16 rungs, 750 mm diameter, 480 mm length, shield 20 mm radial distance to birdcage, 19.5 pF and 40.0 pF capacities in the end rings and rungs). Variations in birdcage dimensions, which were evaluated for one imaging landmark and the 7-month gestation model, included long (600 mm), short (400 mm), and narrow (650-mm diameter) birdcages, as well as a 1.5T birdcage with dimensions identical to that of the reference birdcage. Two separate broadband simulations for the feed-ports I and Q were performed, each yielding a linear B_1 polarization, which were then combined in postprocessing for the desired excitation. A schematic of the possible combinations of the polarizations from I (linear horizontal) and Q (linear vertical) can be found in Figure 2. A relative phase of 90° and amplitude of 1 results in CP mode exposures. Real birdcages may have different locations of the two feeding ports (eg, southwest and southeast below the patient). Although this would change the I-Q graph locations, the results would not be affected, as any elliptical polarization can be achieved with either coil design. Similarly, any cross-coupling between I and Q would be accounted for in the optimization process. Only the CP mode may have

different values in the case of cross-coupling. However, the S12 for all scenarios was below -20 dB. The entire excitation space and its implications on the B_1 polarization can be seen in Figure 2. Simulations, postprocessing, and visualization were performed with Sim4Life Version 2.0 (ZMT, Zurich, Switzerland) and SEMCAD X Version 14.8 (SPEAG, Zurich, Switzerland), with a maximum grid resolution of 2 mm within the active region of the birdcage. The electromagnetic broadband simulation took approximately 1 h per port on hardware-accelerated GPU clusters, whereas one thermal simulation took approximately 10 min.

Worst-Case psSAR10g and RF Shimming Optimization

For the RF shimming-capable two-port birdcages, four different excitation strategies of interest have been analyzed: (a) CP mode as a reference, (b) worst-case local exposure in terms of psSAR10g and temperature in mother and fetus, (c) best uniformity of the B_1^+ field within a specific ROI, and (d) highest average $|B_1^+|$ within the ROI. The formulations and optimization procedures (b) to (d) are based on the *Q*-matrix approach and described in more detail in (3). As the uniformity improvement achieved through (c) may also result in decreased average $|B_1^+|$ (17), excitation strategy (d) corresponding to maximum average $|B_1^+|$ was added. This allows for a balanced tradeoff to be sought, between uniformity and average $|B_1^+|$.

Normalization of all exposure configurations to the maximum allowance of the normal OM (2 W/kg wbSAR) allows comparison of their performance in terms of psSAR10g and average B_1^+. There are only 2 degrees of freedom for the two-port body coil excitation, and the thermal worst-case configuration for the nonlinear thermoregulated model cannot be formulated as a *Q*-matrix. Therefore, the entire I/Q excitation space has been evaluated for the reference scenario by stepping through all possible excitations with sufficiently small step sizes (10° in relative phase, 0.1× to 0.2× in relative amplitude; data points shown in Fig. 4).

Thermoregulation Model and Thermal Simulations

Accurate modeling of local thermoregulation is challenging (8,9) and may be very patient specific. In this study, the thermoregulation model of Laakso et al (8) was widely followed, but with dependence on absolute temperatures instead of temperatures relative to the basal temperature, as described in (9). This yields a more conservative model for skin than in Laakso et al. As no peak temperatures were observed above 43° C, the perfusion model was simplified with skin tissue perfusion saturating at a 16-fold increase as well, discarding the fact that up-regulation would continue for the skin up to an increase factor of 32. The model is defined in Eq. [1] and Figure 3.

In following a conservative approach, local thermoregulation is considered only for the mother (including placenta), but not for the fetus. Heat exchange in the placenta through the umbilical cord is indirectly included through the basal perfusion of blood in the fetus, which is kept at 37°C. The absolute temperature simulations were performed with a Dirichlet thermal boundary condition at major blood vessels and a convection-dependent boundary condition at the interface to external and internal air (h = 6 and 10 W/m^2/K, respectively,

T_{Air} = 25°C), which corresponds to normal breathing and normal clothing with little airflow (18). The metabolic heat generation rate in the fetus was adjusted to yield approximately 0.3°C higher average temperature than that of the mother, as 0.3 to 0.5°C higher temperatures are expected according to (19). During the thermal equilibrium of the simulation before heating, the average temperature of the mother without the skin (as a surrogate for core temperature) was 36.9°C (35.2°C in the skin), with 37.2°C average temperature in the fetus. For a discussion on core and skin temperatures, the reader is referred to (20,21). It has been shown that the core temperature of the mother decreases with progression of the pregnancy, from 37.1°C initially to 36.8°C in the seventh month of gestation (22), for which the worst-case exposure was estimated in this study. The heating was simulated with the maximum allowed exposure (2 W/kg wbSAR) until the thermal steady-state temperature was reached, which was the case after approximately 20– 50 min depending on the exposure scenario.

$$B(T) = B_0 \cdot L_b(T),$$
$$L_b(T) = 1, \qquad T < 37°C$$
$$L_b(T) = 2^{\frac{T-37}{\Delta B}}, \qquad T \geq 37°C, \qquad \Delta B = 1.6$$
$$\text{upper limit } L_b : 16$$

[1]

where $B(T)$ is the perfusion rate at temperature T, $L_b(T)$ is the local temperature dependent multiplier, B_0 is the basal perfusion at or below 37°C, and ΔB is the local vasodilation parameter.

RESULTS

SAR Evaluations

The model corresponding to 7 months' gestation within the reference birdcage and in the fetus imaging landmark is hereafter called the *reference scenario* and is tagged with an asterisk (*). Except for the short 400-mm coil, this was found to be the worst-case configuration. This reference scenario is covered in more detail in Figure 4, which shows the psSAR10g for the mother (including the fetus) and for the fetus alone, for the entire I/Q excitation space. The patterns for mother and fetus are nearly opposite: A decrease in psSAR10g for the mother is generally accompanied by an increase in SAR for the fetus. When moving from CP to the typical RF shimming region, the psSAR10g decreases for the mother but increases for the fetus (green arrows). The psSAR10g of the fetus increases from 7.4 W/kg at CP to a maximum of 21.3 W/kg with linear polarization, with the RF shimmed values between approximately 10 to 16 W/kg for the different ROIs in this imaging position.

The same behavior is observed in Figure 5, where different influencing factors—(a) imaging landmark, (b) gestation, and (c) body coil type—are investigated. Although RF-shimmed excitations lead in most cases to lower psSAR10g than with CP in the mother (gray shaded area is below the black dashed line), the exposure of the fetus is always higher with RF shimming compared with CP. The highest psSAR10g is found in the reference scenario (21.3 W/kg), with the exception of the short 400-mm birdcage (see “Discussion”). The psSAR10g values reach up to >40 W/kg in the mother. Fetal exposure at 1.5T CP is higher than at 3T CP. However, RF shimmed excitations—which are typically implemented at 3T but not at 1.5T—lead to higher exposures at 3T. Values for selected SAR results can be found in Table 1. Figure 5 also shows the average SAR values, which can reach >3 W/kg in the fetus and >12 W/kg in the amniotic fluid.

The psSAR10g values for the neonate (infant without the mother) did not exceed 12.7 W/kg for a wbSAR of 2 W/kg (normal OM) in any excitation regime (not depicted). Compared with adult patients this is approximately 4 times less, because of the small body dimensions, and in good agreement with the estimation in (23).

RF Shimming Performance

To estimate a typical RF shimming excitation region, all I/Q excitations with best B_1^+ uniformity and highest $|B_1^+|$ in the respective ROI were determined and are depicted in Figure 6a. The corresponding ROIs are defined in Figure 1. A stronger horizontal B_1 polarization is preferable for both best field uniformity and highest $|B_1^+|$ (with, on average, a relative amplitude of 0.55×, and a relative phase of 118°). The RF shimming parameter space for the reference scenario (Fig. 6) shows a $CV(B_1^+)$ within the fetus of 16% (best shimming) and 18% (CP mode). A mean B_1^+ level of 2.32 μT (highest average $|B_1^+|$) and 2.02 μT (CP) can be applied in normal OM. Thus, imaging can gain up to ~12% in image uniformity and 0.8 dB in transmit efficiency in the reference scenario compared with CP, and the fetus as ROI. These RF shimming enhancements on the order of 10% are lower than the more asymmetric geometries of nonpregnant patients, in which 32% enhancement can be expected on average (3). This is because of the quasi-spherical shape of the late-gestation pregnant models. However, when including all investigated scenarios and ROIs, the gain in image uniformity still averages to 29%.

Temperature Increase

The numerically derived steady-state temperature distributions in four excitation configurations (CP mode, best shimming, worst-case psSAR10g for the mother and for the fetus) are shown in Figure 7, all for the reference scenario. The worst-case excitation for psSAR10g in the mother leads to a rather low peak temperature of the fetus (T < 37.8°C), whereas CP (38.4°C) and RF shimming (39.6°C) increase the local fetal temperature significantly. Finally, the worst-case exposure in the fetus, depicted in Figure 7, is reached with a linear horizontal polarization (40.8°C). The high temperatures in the fetus are a result of the generally higher SAR in the amniotic fluid, the temperature of which is also higher than in the fetus, because of the absence of perfusion. The constriction of the amniotic fluid (Fig. 7) leads to a pronounced hotspot and a peak temperature of 41°C, which causes a peak temperature of 40.8°C in the neighboring fetal tissues. This estimated peak temperature is a

conservative estimation, as there is no motion of the amniotic fluid modeled. The time to reach the steady-state condition is on the order of 20–50 min. An overview of the temperatures attained for the selected scenarios is given in Table 1.

The maximum increase of the average temperature was from 36.9 to 37.4°C in the mother, from 37.2 to 37.8°C in the fetus, and from 37.2 to 38.3°C in the amniotic fluid. The average temperature of the fetus was always 0.14 to 0.54°C higher than in the mother.

For the neonate (only the newborn in the scanner, without mother) in normal OM, the peak temperature reaches 39.1°C with thermoregulation and 39.8°C in its absence. The difference remains small, as the level of exposure corresponds to that at the onset of thermoregulation (8). However, scanning in the first level controlled OM—which is not prohibited for neonates or premature infants according to the IEC standard—may result in temperatures of up to 43.1°C in the absence of local thermoregulation.

Numerical Uncertainty

To estimate the upper/lower bounds and parameter sensitivities, the uncertainty of our results, ie, psSAR10g and temperature increase for the normal OM (wbSAR = 2 W/kg), were determined based on the modeling parameter uncertainties for the worst-case fetal exposure scenario, according to the concept of NIST TN1297 (24). The following uncertainties were assumed for the psSAR10g modeling parameters: simulation convergence (double simulation time); model discretization (1.5 mm, 3 mm voxel size); 10% variation in all dielectric properties, dielectric contrast, and density contrast; and age-adjusted dielectric properties. The dielectric and density contrast refers to adjusting the properties only for one tissue at a time or for the fetus only. As the exposure is normalized to wbSAR, the dielectric contrast has a large influence. For the thermal parameters, the following uncertainties were assumed: convergence and discretization (same as for SAR), 10% in specific heat capacities of tissues and blood, 20% in metabolic heat generation and thermal conductivity, 50% in thermal boundary conditions, and tissue perfusion. The age-adjusted tissue properties assessed in (16) were also included.

The combined root-sum-square (RSS) uncertainty accumulates to 0.4 dB (~9%) for psSAR10g, and 1.4 dB (~30%) in temperature increase, similar to the results presented in (9). The largest contributions to the uncertainty originate from dielectric and density contrast in the electromagnetic simulation, and from blood perfusion and model discretization in thermal simulation. The resulting uncertainty intervals can be found in Table 1.

DISCUSSION

For an RF shimmed birdcage (two-port excitation) within the normal OM (wbSAR = 2 W/kg), the psSAR10g can reach values above 40 W/kg in the mother, and up to 24 W/kg in the fetus, as well as an average SAR of >3 W/ kg in the fetus and >12 W/kg in the amniotic fluid (Fig. 5). Although the values for CP do not differ greatly between 1.5T and 3T excitations, RF shimming—typically not implemented at 1.5T—may worsen the fetal exposure significantly. Therefore, the previous assumption that local exposure in the mother

is at least several times higher than in fetal tissues (6) does not hold for RF shimmed excitations, in which the values actually may become similar (see Table 1).

Emerging technologies including pTx excitations (more than two channels) and dynamic RF shimming with varying waveforms per channel (25) are beyond the scope of this study, but may be part of future research activities.

According to the latest (2015) version of IEC 60601-2-33 (4), the “fetus is considered as part of the general public” (Section 201.7.9.2.101 u)). Thus, the exposure should be in compliance with corresponding standards such as ICNIRP (26). However, the basic restrictions of ICNIRP are as low as wbSAR = 0.08 W/kg and psSAR10g = 2–4 W/kg, which is exceeded for the fetus in all investigated scenarios in normal OM by at least a factor of 2 (even for low-SAR RF shimming in the third month of gestation models). For the selected scenarios in Table 1, the basic restrictions are exceeded by a factor of 6–35, or a factor of 1.3–5.3 when only considering psSAR limits. This obvious contradiction of allowing normal OM for pregnant patients, which may result in fetal exposures above the limits for general public, needs to be resolved.

Our estimated peak temperature (pT) value for the CP excitation (38.4°C) corresponds well to the 38.7°C derived in a similar study for a CP 3T birdcage (6), in which the tissue properties for the fetus were homogenous. However, when the pT for the worst-case fetus exposure (40.8° C in this study) is evaluated with the same homogenous tissue properties from (6), only 39.1° C is reached. The major reason for this difference is the different value for perfusion in the fetal body of 262 ml/ min/kg (approximated from 4.59 kg/m^3/s, (6)), whereas the tissues in the fetal hotspot in this study are perfused at a rate of only 32–106 ml/min/kg. To a lesser extent (accounting for approximately 25% of the difference), the homogenous tissue properties lead to a lower eddy current density in the amniotic fluid constriction depicted in Figure 7. These points emphasize the need for accurate anatomical modeling and tissue assignment.

The reference scenario has been defined with the reference coil, as it appeared to us that it is the most realistic length for a 3T coil. The comparison to other coil types has been added for completeness. However, the short coil induces slightly higher SAR and temperatures values: 24.3 instead of 21.3 W/kg in fetal psSAR10g and 41.2° C instead of 40.8° C in fetal peak temperature.

The proposed thermal dose limit of CEM43 = 2 min for the fetus (27) translates to approximately 40 min at 40.8° C (our estimated maximum temperature in normal OM). Thus, the limit is reached in the worst-case configuration after approximately 90 min of constant maximum exposure, including the initial heating phase of approximately 40–50 min. However, because of the frequent fetal movements, the hotspot is unlikely to remain at the same location for a prolonged duration. Ideally, a whole set of fetal postures would be examined to create a posture-averaged hotspot map, but the necessary set of models is not yet available. Additionally, SAR is very unlikely to remain at the maximum allowance for 90 min, as a result of frequent interruptions and different scan sequences (28). The situation with the maximum and a realistic exposure is illustrated in Figure 8, which shows the effect

of SAR to the transient peak temperature of the fetus and the accumulation of thermal dose. Prolonged scans with high SAR constitute the highest risk of thermal damage.

Compared with the worst-case exposures with linear horizontal excitation, a restriction to CP mode for pregnant patients would reduce the fetal average SAR and psSAR10g exposure by a factor of at least 1.8 for all investigated scenarios (on average by a factor of 2.7). Compared with RF shimming excitations, the corresponding reduction in CP mode would be at least a factor of 1.2 (on average a factor 1.8). This average reduction of 45% in fetal exposure would come at the cost of a 13% smaller mean B_1^+ level and a 12% decrease in $CV(B_1^+)$.

Exposure in first level controlled OM would lead to fetal temperatures of >43° C in our worst-case RF shimming scenario, reaching the thermal dose limit after approximately 15 min. Thus, scanning above the normal OM cannot be recommended, which is in agreement with (6).

The ability of neonates, particularly preterm infants, to thermoregulate may be highly compromised (29). Exposure to the full allowance of the first level controlled OM may cause local temperatures of up to 43.1° C in neonates (infant without the mother). Thus, it may be advisable to limit exposures to the normal OM for neonates, especially as this would not change clinical practice, in which wbSAR levels typically remain below 1 W/kg (23).

CONCLUSIONS

It would appear from these simulations that two-port RF shimming at 3T can significantly increase the fetal exposure in pregnant women. Further research will be required to derive a very robust safety management. The previous assumption that local exposure in the mother is at least several times higher than in fetal tissues does not hold for RF shimmed excitations. Restriction to the CP mode, which significantly reduces (by a factor of ~2–3) fetal SAR exposure compared to linear-horizontal polarization modes, may be advisable. Exposure of pregnant women and neonates above the normal OM cannot be recommended for RF shimmed excitations. This study emphasizes the need for anatomical models with nonhomogenous tissue properties and the necessity for further work that includes more anatomical models to cover the pregnant patient population with different anatomies, body metrics (eg, BMI), fetal positions, and placenta locations.

Acknowledgments

This study was supported in part by the MRIneo project. The work of J. Córcoles was supported by CICYT, Spain (contract TEC2013-47106-C3-2-R) and Banco Santander-UAM (contract 2015/ASIA/03). The mention of commercial products, their sources, or their use in connection with material reported herein is not to be construed as either an actual or implied endorsement of such products by the Department of Health and Human Services.

References

1. Pugash D, Brugger PC, Bettelheim D, Prayer D. Prenatal ultrasound and fetal MRI: the comparative value of each modality in prenatal diagnosis. Eur J Radiol. 2008; 68:214–226. [PubMed: 18790583]
2. Bulas D, Egloff A. Benefits and risks of MRI in pregnancy. Semin Perinatol. 2013; 37:301–304. [PubMed: 24176150]

3. Murbach M, Neufeld E, Cabot E, Zastrow E, Juan C, Kainz W, Kuster N. Virtual population-based assessment of the impact of 3 Tesla radiofrequency shimming and thermoregulation on safety and B_1^+ uniformity. Magn Reson Med. 2015; doi: 10.1002/mrm.25986
4. IEC. Part 2-33: Particular requirements for the basic safety and essential performance of magnetic resonance equipment for medical diagnosis. 3.2. CSV; 2015. Medical electrical equipment. IEC 60601-2-33:2010+AMD1:2013+AMD2:2015
5. Murbach M, Cabot E, Neufeld E, Gosselin M-C, Christ A, Kuster N. Local SAR enhancements in anatomically correct children and adult models as a function of position within 1.5 T MR body coil. Prog Biophys Mol Biol. 2011; 107:428–433. [PubMed: 21964524]
6. Hand JW, Li Y, Hajnal JV. Numerical study of RF exposure and the resulting temperature rise in the foetus during a magnetic resonance procedure. Phys Med Biol. 2010; 55:913–930. [PubMed: 20090188]
7. Wu D, Shamsi S, Chen J, Kainz W. Evaluations of specific absorption rate and temperature increase within pregnant female models in magnetic resonance imaging birdcage coils. IEEE Trans Microw Theory Tech. 2006; 54:4472–4478.
8. Laakso I, Hirata A. Dominant factors affecting temperature rise in simulations of human thermoregulation during RF exposure. Phys Med Biol. 2011; 56:7449–7471. [PubMed: 22080753]
9. Murbach M, Neufeld E, Capstick M, Kainz W, Brunner DO, Samaras T, Pruessmann KP, Kuster N. Thermal tissue damage model analyzed for different hole-body SAR and scan durations for standard MR body coils. Magn Reson Med. 2014; 71:421–431. [PubMed: 23413107]
10. Kellogg DL. In vivo mechanisms of cutaneous vasodilation and vasoconstriction in humans during thermoregulatory challenges. J Appl Physiol. 2006; 100:1709–1718. [PubMed: 16614368]
11. Graven-Nielsen T, Arendt-Nielsen L, Mense S. Thermosensitivity of muscle: high-intensity thermal stimulation of muscle tissue induces muscle pain in humans. J Physiol. 2002; 540:647–656. [PubMed: 11956350]
12. Piontelli, A. Development of normal fetal movements: the last 15 weeks of gestation. Springer Milan; Italy: 2015.
13. Christ A, Kainz W, Hahn EG, et al. The virtual family—development of surface-based anatomical models of two adults and two children for dosimetric simulations. Phys Med Biol. 2010; 55:N23–N38. [PubMed: 20019402]
14. Gosselin M-C, Neufeld E, Moser H, et al. Development of a new generation of high-resolution anatomical models for medical device evaluation: the Virtual Population 3.0. Phys Med Biol. 2014; 59:5287–5303. [PubMed: 25144615]
15. Gabriel S, Lau R, Gabriel C. The dielectric properties of biological tissues II: Measurements in the frequency range 10 Hz to 20 GHz. Phys Med Biol. 1996; 41:2251–2269. [PubMed: 8938025]
16. Peyman A, Gabriel C, Grant EH, Vermeeren G, Martens L. Variation of the dielectric properties of tissues with age: the effect on the values of SAR in children when exposed to walkie-talkie devices. Phys Med Biol. 2009; 54:227–241. [PubMed: 19088390]
17. Ibrahim TS, Tang L. Insight into RF power requirements and B_1 field homogeneity for human MRI via rigorous FDTD approach. J Mag Res Imag. 2007; 25:1235–1247.
18. Bernardi P, Cavagnaro M, Pisa S, Piuzzi E. Specific absorption rate and temperature elevation in a subject exposed in the far-field of radio-frequency sources operating in the 10–900-MHz range. IEEE Trans Biomed Eng. 2003; 50:295–304. [PubMed: 12669986]
19. Asakura H. Fetal and neonatal thermoregulation. J Nippon Med Sch. 2004; 71:360–370. [PubMed: 15673956]
20. Aschoff J, Wever R. Kern und Schale im Wärmehaushalt des Menschen. Naturwissenschaften. 1958; 45:477–485.
21. Taylor NAS, Tipton MJ, Kenny GP. Considerations for the measurement of core, skin and mean body temperatures. J Therm Biol. 2014; 46:72–101. [PubMed: 25455943]
22. Hartgill TW, Bergersen TK, Pirhonen J. Core body temperature and the thermoneutral zone: a longitudinal study of normal human pregnancy. Acta Physiol. 2011; 201:467–474.
23. Malik SJ, Beqiri A, Price AN, Teixeira JN, Hand JW, Hajnal JV. Specific absorption rate in neonates undergoing magnetic resonance procedures at 1.5 T and 3 T. NMR Biomed. 2015:344–352. [PubMed: 25594939]

24. Taylor, BN., Kuyatt, CE. Guidelines for evaluating and expressing the uncertainty of NIST measurement results. NIST; Gaithersburg, MD: 1994. Technical Note 1297

25. Guérin B, Gebhardt M, Serano P, Adalsteinsson E, Hamm M, Pfeuffer J, Nistler J, Wald LL. Comparison of simulated parallel transmit body arrays at 3 T using excitation uniformity, global SAR, local SAR, and power efficiency metrics. Magn Reson Med. 2015; 73:1137–1150. [PubMed: 24752979]

26. ICNIRP. Guidelines for limiting exposure to time-varying electric, magnetic, and electromagnetic fields (up to 300 GHz). Heal Phys. 1998; 74:494–522.

27. van Rhoon GC, Samaras T, Yarmolenko PS, Dewhirst MW, Neufeld E, Kuster N. CEM43°C thermal dose thresholds: a potential guide for magnetic resonance radiofrequency exposure levels? Eur Radiol. 2013; 23:2215–2227. [PubMed: 23553588]

28. Brugger PC, Prayer D. Actual imaging time in fetal MRI. Eur J Radiol. 2012; 81:e194–e196. [PubMed: 21345632]

29. Arthurs OJ, Edwards A, Austin T, Graves MJ, Lomas DJ. The challenges of neonatal magnetic resonance imaging. Pediatr Radiol. 2012; 42:1183–1194. [PubMed: 22886375]

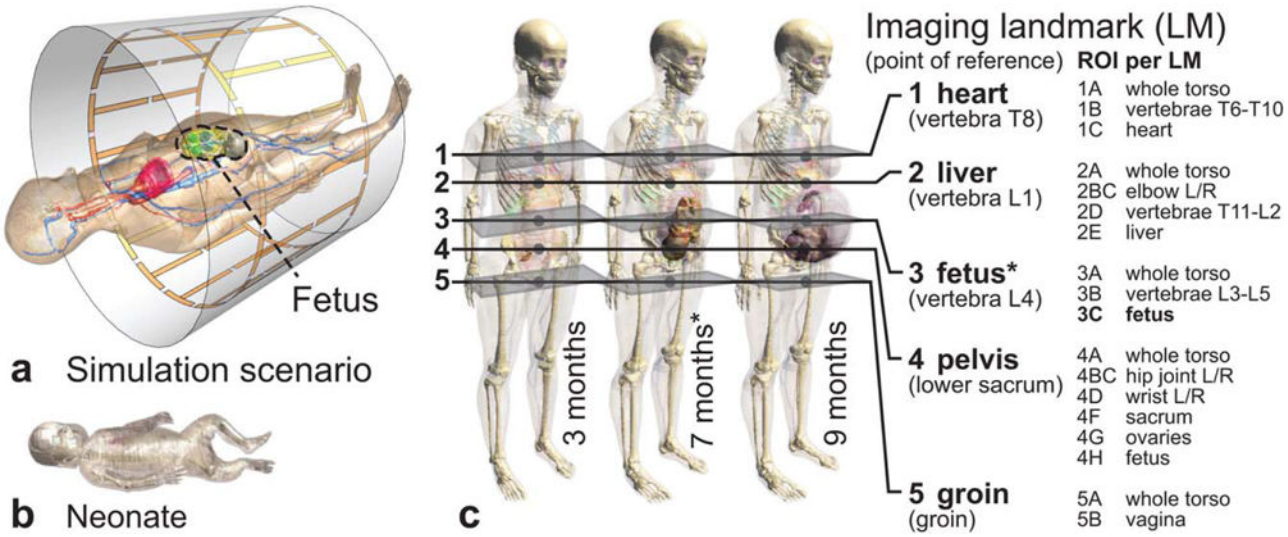

FIG. 1.

(a) Simulation scenario within the reference birdcage. (b) Neonate model included in the study. (c) Three anatomical pregnant women models at the third, seventh, and ninth month of gestation, with the evaluated imaging landmarks and corresponding ROIs per landmark. Many points of reference and ROIs are based on the locations of specific thoracic (T) and lumbar (L) vertebrae.

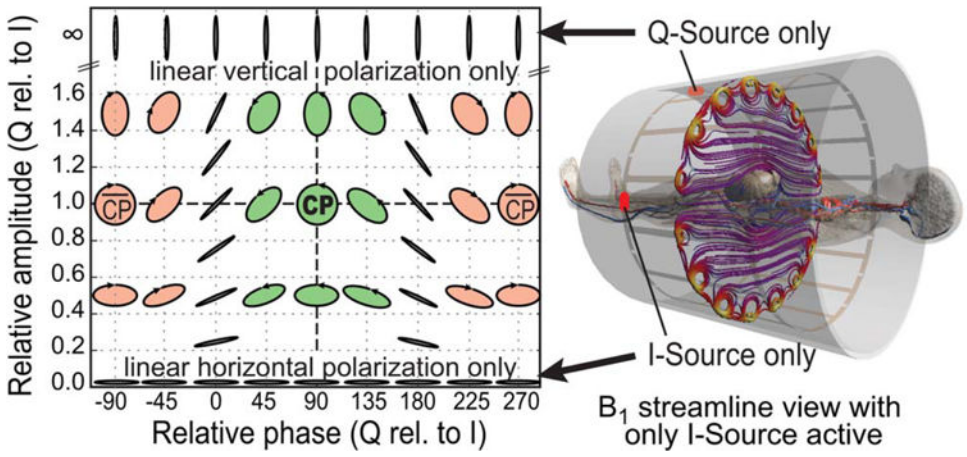

FIG. 2.

I/Q excitation space. CP with a relative amplitude of 1 and a relative phase of 90°. Linear polarization occurs when only I is active (horizontal, depicted on the right) or only Q is active (vertical), or with a relative phase of 0/180° (arbitrary polarization angles). The graph is for visualization purposes only and does not correspond to data points actually simulated.

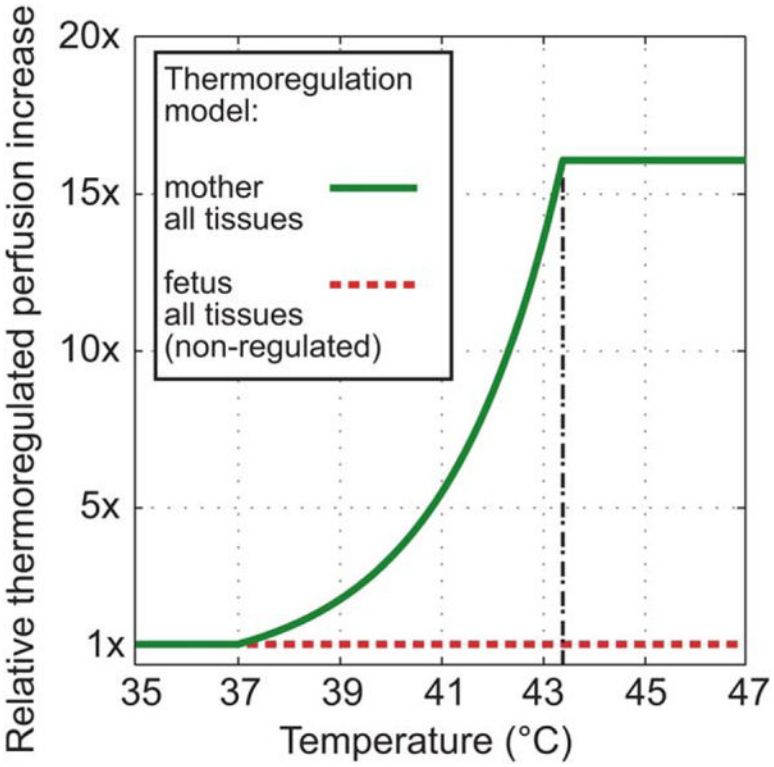

FIG. 3.

Applied local thermoregulation models. Relative blood perfusion increases as a function of absolute tissue temperature. Body-parts with no perfusion, eg, the amniotic fluid, are therefore not affected. Perfusion in the fetus is assumed to be constant.

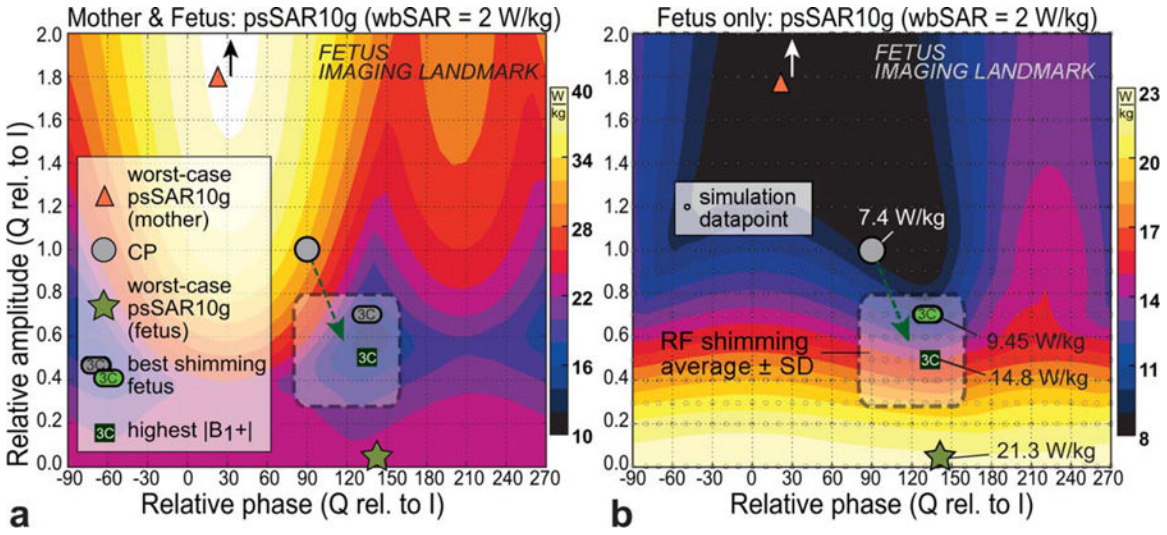

FIG. 4.

psSAR10g within the RF shimming parameter space for the reference scenario, for the mother including the fetus (a) and the fetus only (b). When compared with CP, the typical RF shimming excitations tend to lower the psSAR10g in the mother but increase SAR in the fetus (see dashed green arrow). Worst-case psSAR10g for the mother is outside of the graph at 2.2× and 30° (black/white arrows). The typical RF shimming region is indicated (from Fig. 6). The simulation data points underlying these interpolated graphs are shown in (b).

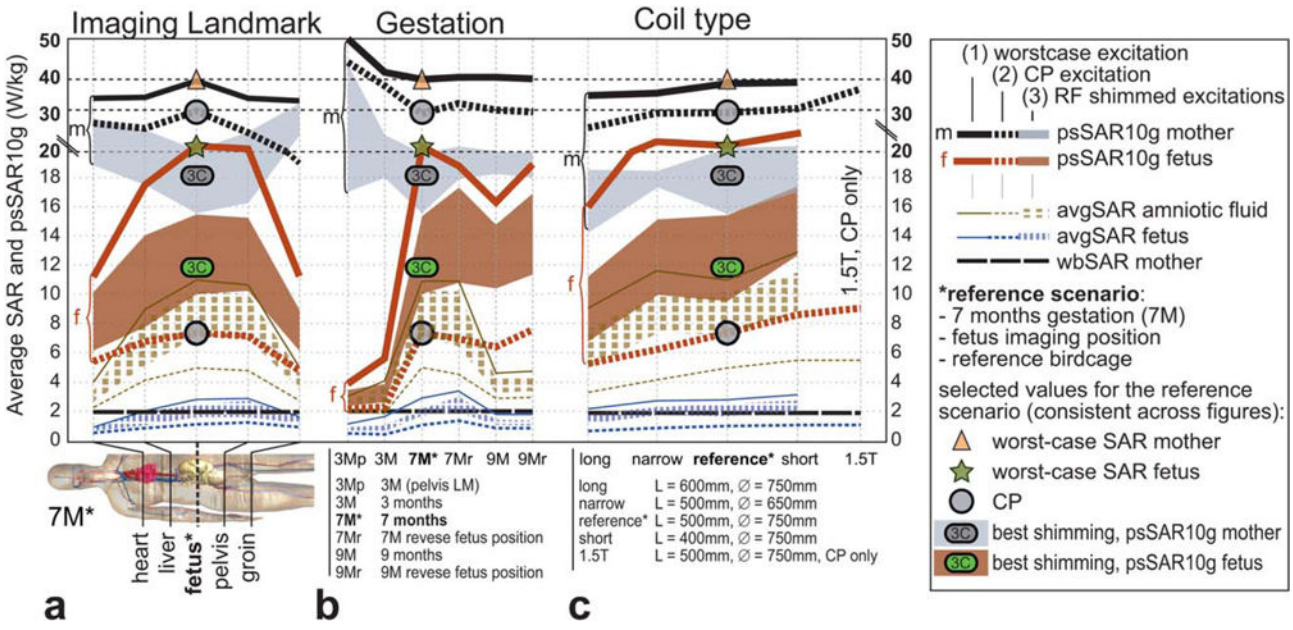

FIG. 5.

Influence of imaging landmark, stage of gestation, and coil type on the psSAR10g and average SAR of mother, fetus, and amniotic fluid. (a) Fetus-centered imaging landmark (*) indicates the highest SAR levels for the fetus. (b) Model at the seventh month of gestation (7M*) has a higher SAR than the other pregnant models. (c) Four body coil dimensions at 3T and one at 1.5T coil in CP mode only; only the short coil induces more SAR than the reference* coil. Triangle, circle, and star signs correspond to the values in Figure 4 and are consistent with the other figures.

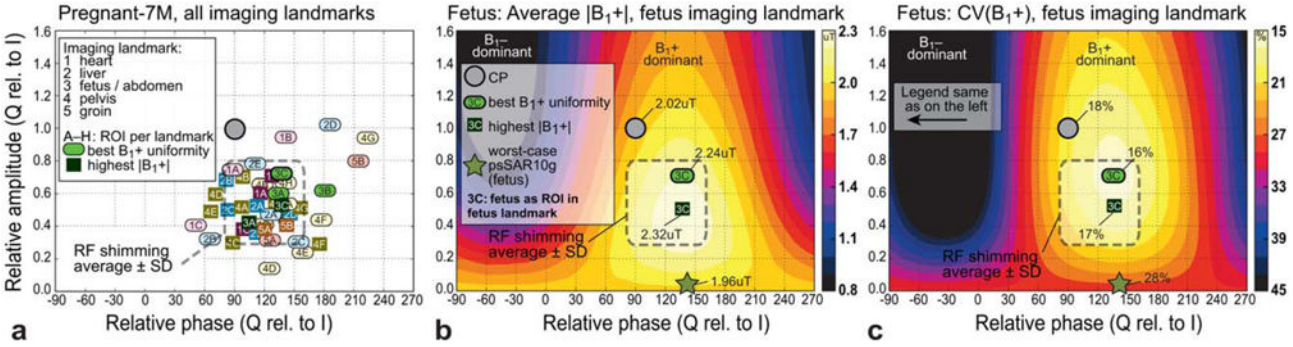

FIG. 6.

(a) RF shimming excitations leading to the best uniformity of B_1^+, and the highest average $|B_1^+|$. The typical RF shimming excitation region is indicated as the average ± standard deviation of the relative amplitudes and phases. (b, c) Average $|B_1^+|$ and CV (B_1^+) for the fetus as ROI (3C) in the fetus-centered imaging landmark. ROIs are defined in Figure 1.

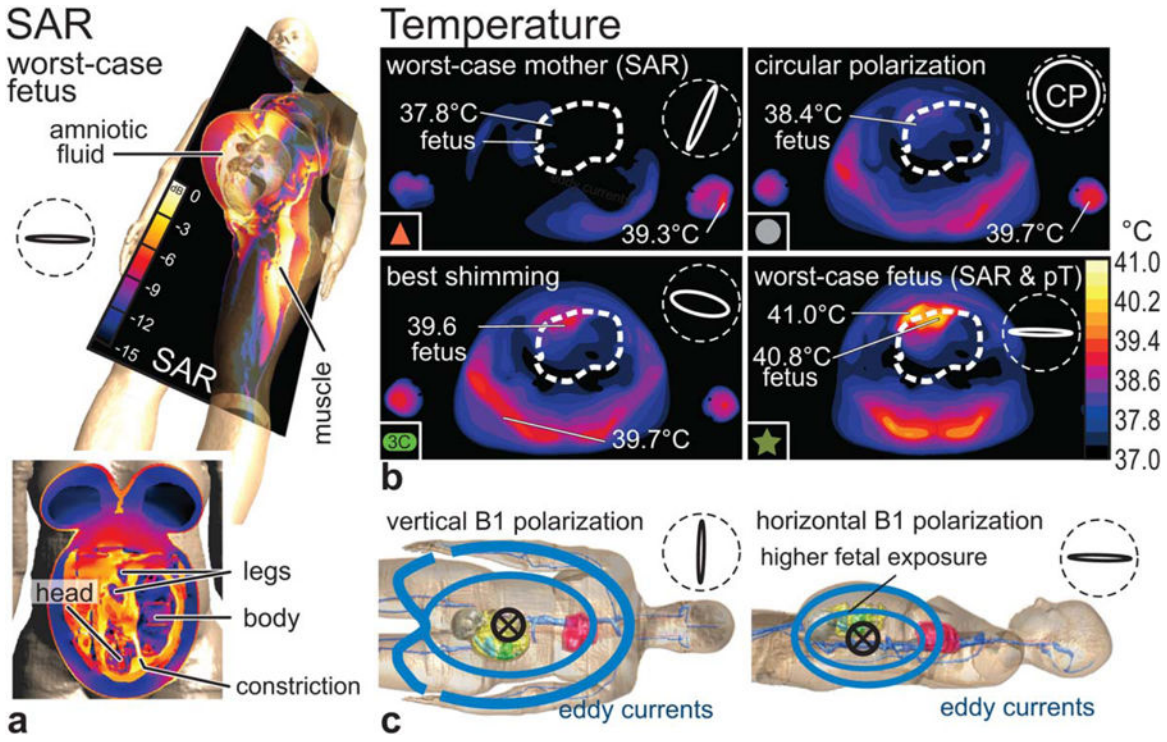

FIG. 7.

(a) SAR distribution for worst-case fetus excitation in inclined and frontal slice view. The constriction of amniotic fluid between the head and shoulder of the fetus leads to a hotspot. (b) Temperature distribution at steady state (after 50 min) in transversal slice view, with indicated peak temperatures (pT) for mother and fetus. Vertical B_1 polarizations lead to lateral exposures, whereas horizontal polarization deposit energy at the back and in the region of the fetus. Polarization ellipses are indicated within dashed circles (along bore-sight). All evaluations were made with the reference scenario. Symbols (eg, red triangle) are consistent with the other figures. (c) Illustration of basic eddy current patterns.

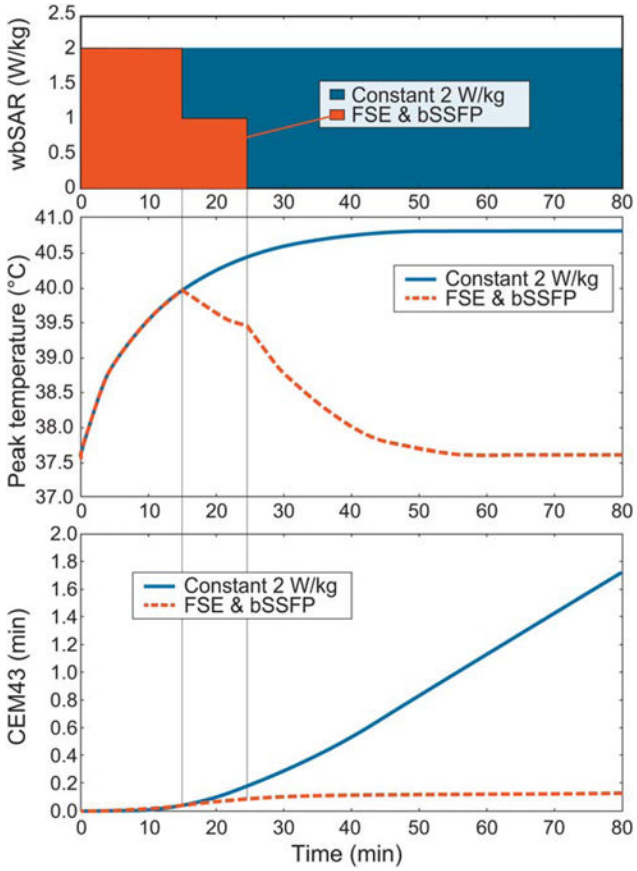

FIG. 8.

Illustration of the relationships between wbSAR, transient peak temperature of the fetus (pT), and thermal dose accumulation (CEM43). The investigated worst-case scenario (constant 2 W/kg wbSAR) is shown together with a representative clinical scan sequence of 2 W/kg wbSAR for 15 min (eg, a single-shot fast spin-echo (FSE) acquisition) followed by 10 min of only 1 W/ kg wbSAR (eg, a balanced steady-state free precession (bSSFP) sequence). The proposed threshold for thermal damage of CEM43 = 2 min would be reached after 90 min of constant 2 W/ kg wbSAR.

Table 1

Summary of SAR, Average Temperature, and Peak Temperature at steady state (SS) for Selected Configurations in the Reference Scenario

	avgSAR (W/kg)			psSAR10g (W/kg)			avgT at SS (°C)			pT at SS (°C)		
Configuration	**Mother**	**Fetus**	**Amni.**	**Mother**	**Fetus**	**Amni.**	**Mother**	**Fetus**	**Amni.**	**Mother**	**Fetus**	**Amni.**
CP values from Hand et al (6) *for comparison*	*2.0*	*1.05*	*2.74*	*> 20.0*	*5.3*	*13.1*	*> 37.3*	*37.6*	*39.6*	*> 38.9*	*38.7*	*40.1*
CP	2.0	1.13	4.94	29.6	7.4	8.0	37.3	37.5	37.6	39.7	38.4	38.3
WC mother (SAR)	2.0	0.52	2.34	39.9	6.3	8.6	37.1	37.3	37.4	39.3	37.8	37.8
Best shim, ROI: fetus (min. CV(B_1^+))	2.0	1.62	6.62	18.5	9.45	10.1	37.4	37.6	38.0	39.7	39.6	39.6
WC fetus	2.0	**2.77**	11.0	22.7	**21.3**	22.6	37.3	**37.8**	38.3	41.0	**40.8**	41.0
Uncertainty interval for the fetus in the line above ***(bold)***		***(2.47; 3.11)***			***(19.5; 23.3)***			***(37.5; 38.1)***			***(39.8; 42.4)***	

Note: The uncertainty interval for fetal worst-case exposure (bold) is stated on the last row. The first row states the values from Hand et al (6), in which the sixth month of gestation NICT model was used with homogenous tissue properties for the fetus. avgT, average temperature; pT, peak temperature; SS, steady state; WC, worst-case.